Detailed modelling of the susceptibility of a thermally populated, strongly driven circuit-QED system

Detailed modelling of the susceptibility of a thermally populated, strongly driven circuit-QED system

Anton Frisk Kockum[1,3]**, Martin Sandberg**[2,3]**, Michael R Vissers**[2]**, Jiansong Gao**[2]**, Göran Johansson**[1] **and David P Pappas**[2,4]

[1] Department of Microtechnology and Nanoscience, Chalmers University of Technology, SE-41296 Göteborg, Sweden
[2] National Institute of Standards and Technology, Boulder, CO 80305, USA

E-mail: david.pappas@nist.gov

Abstract
We present measurements and modelling of the susceptibility of a 2D microstrip cavity coupled to a driven transmon qubit. We are able to fit the response of the cavity to a weak probe signal with high accuracy in the strong coupling, low detuning, i.e., non-dispersive, limit over a wide bandwidth. The observed spectrum is rich in multi-photon processes for the doubly dressed transmon. These features are well explained by including the higher transmon levels in the driven Jaynes–Cummings model and solving the full master equation to calculate the susceptibility of the cavity.

Cavity quantum electrodynamics (CQED) studies the interaction between electromagnetic fields and atoms [1, 2]. To prolong the interaction time, the electromagnetic field is localized using a resonant cavity. The interaction can be observed by allowing an atom to pass through the cavity and then performing measurements on the atom itself, or by probing the susceptibility of the cavity. In recent years, the field of CQED has been expanded to include superconducting electrical circuits, where it has become known as circuit quantum electrodynamics (cQED) [3, 4].

In cQED, the Josephson junction can be used as a nonlinear inductor, allowing for the construction of anharmonic oscillators, or 'artificial atoms', with engineered energy levels. In most applications, these artificial atoms are used as qubits, with only the two lowest energy levels considered [5].

The qubits can be coupled (capacitively or inductively) to high-quality-factor microwave transmission line resonators. One attractive feature of cQED is that the qubit position is fixed by fabrication. In addition, their extended size creates a large dipole moment. This together with the concentrated fields of one-dimensional cavities allows for very strong coupling between the qubit and the (microwave) field [6].

The large size of the qubits also makes the interaction with the environment stronger, leading to dephasing and relaxation. In the first generation of these devices, the coherence times were only a few nanoseconds [7]. Today, due to careful engineering of the circuits and the environment, coherence times of the order 10 μs all the way up to 55 μs can reliably be achieved [8–12]. The fact that the systems can be engineered, and the relative ease with which these devices can be operated, makes cQED a very attractive system for the study of Jaynes–Cummings physics.

In this work, we present measurements and modelling of the susceptibility of a coherent cQED circuit driven over a wide range of frequencies and drive powers. The circuits are fabricated primarily from low loss, stoichiometric titanium nitride (TiN) on high purity intrinsic silicon (Si) [13]. The qubit and the microstrip resonant cavity are fabricated in a planar geometry as described in [8].

The qubit is of the transmon type [14]. It consists of a small Josephson junction shunted by a capacitor formed by two large paddles; see figures 1(a) and (b). The large structure acts to dilute the otherwise high interface losses [15–17], allowing for long coherence times. Radiation losses in this design are

---

[3] These authors contributed equally to this work.
[4] Author to whom any correspondence should be addressed.

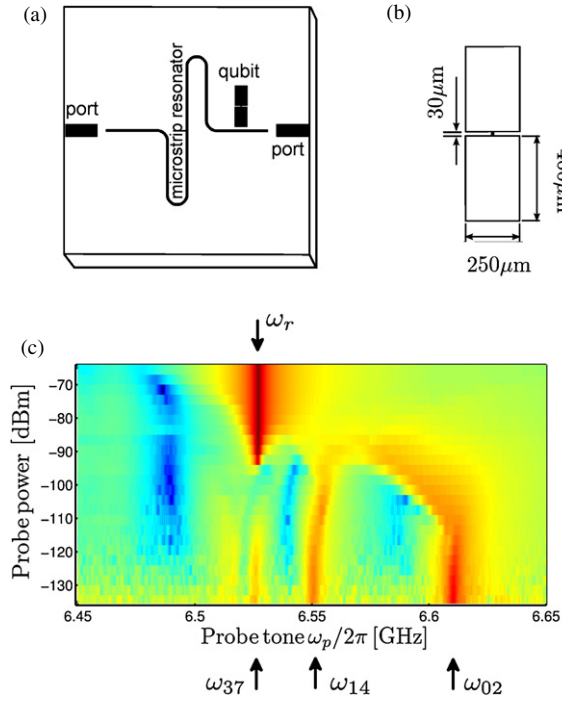J. Phys. B: At. Mol. Opt. Phys. **46** (2013) 224014

A F Kockum *et al*

Figure 1. (a) Chip layout, a single qubit coupled to a microstrip resonator. (b) Dimensions of the qubit. (c) Measured transmission for different probe powers (logarithmic colour scale, where red indicates close to full transmission and blue close to zero transmission). At high probe power only the bare resonator is visible (indicated by ω_r). As we lower the probe power, multiple shifted peaks appear (indicated by ω_{37}, ω_{14} and ω_{02}), corresponding to transitions of the dressed qubit–resonator system.

Table 1. Eigenstate energies of the single-dressed resonator–qubit system. The first index in the ket is the resonator, and the second the qubit. Five resonator states (0, 1, 2, 3, 4) and five transmon states (g, e, f, h, i) were used in the model.

Singly dressed state	E/h (GHz)	State
$\lvert 0, g\rangle$	0	$\lvert\mathbf{0}\rangle$
$-.90\lvert 0, e\rangle + .43\lvert 1, g\rangle$	6.104	$\lvert\mathbf{1}\rangle$
$-.43\lvert 0, e\rangle + .90\lvert 1, g\rangle$	6.616	$\lvert\mathbf{2}\rangle$
$-.91\lvert 0, f\rangle + .40\lvert 0, e\rangle - .11\lvert 2, g\rangle$	12.003	$\lvert\mathbf{3}\rangle$
$-.39\lvert 0, f\rangle + .74\lvert 0, e\rangle - .55\lvert 2, g\rangle$	12.660	$\lvert\mathbf{4}\rangle$
$-.14\lvert 0, f\rangle + .54\lvert 0, e\rangle - .83\lvert 2, g\rangle$	13.225	$\lvert\mathbf{5}\rangle$
$-.93\lvert 0, h\rangle - .36\lvert 1, f\rangle + .09\lvert 2, e\rangle - .02\lvert 3, g\rangle$	17.650	$\lvert\mathbf{6}\rangle$
$-.35\lvert 0, h\rangle - .76\lvert 1, f\rangle + .52\lvert 2, e\rangle - .17\lvert 3, g\rangle$	18.535	$\lvert\mathbf{7}\rangle$
$-.12\lvert 0, h\rangle - .50\lvert 1, f\rangle + .60\lvert 2, e\rangle - .61\lvert 3, g\rangle$	19.218	$\lvert\mathbf{8}\rangle$
$-.04\lvert 0, h\rangle - .21\lvert 1, f\rangle + .60\lvert 2, e\rangle - .77\lvert 3, g\rangle$	19.829	$\lvert\mathbf{9}\rangle$

suppressed by placing the qubit above the superconducting ground plane of the microstrip resonator. Although the electric field strength generated by the microstrip resonator is weaker than that of typical coplanar waveguide resonators used in cQED systems, the large pad geometry still allows for strong coupling between the qubit and the resonator.

The sample was mounted inside a Cu sample box with the conducting backplane of the device electrically connected to the box. It was measured in an adiabatic demagnetization refrigerator (ADR) at a base temperature ≈ 50 mK.

The characterization of the cQED system was performed by measuring the transmission coefficient S_{21} of a microwave signal at probe frequency $\omega_p/2\pi$. At high probe powers, the bare resonator's fundamental mode was observed at 6.53 GHz, as shown in figure 1(c) [18–20]. The quality factor $Q = 5300$ was extracted from a similar sample without a transmon. As the probe power was decreased, the bare resonance disappeared from the spectrum, and instead a dispersively shifted resonance appeared; see figure 1(c).

From the measured spectrum, we extract a qubit $\lvert g\rangle \leftrightarrow \lvert e\rangle$ transition frequency of $\omega_{ge}/2\pi \approx 6.2$ GHz, a charging energy $E_C/h \approx 285$ MHz and a qubit–resonator coupling $g/2\pi \approx 190$ MHz. Since $g/\Delta \sim 1$, where Δ is the detuning between the resonator and the first qubit transition, the system is not in the dispersive regime. This strongly coupled system is interesting because it allows for the study of dressed qubit states and the interaction between the qubit and the environment. A similar

system has previously been studied [21], but here we model the full system response.

To model the system, we use the multilevel Jaynes–Cummings Hamiltonian [14] for the transmon–resonator system (i.e. a singly dressed transmon),

$$H_{JC} = \hbar\omega_r a^\dagger a + \hbar \sum_{j=0}^{N_t-1} \omega_j \lvert j\rangle\langle j\rvert$$
$$+ \hbar \sum_{j=0}^{N_t-1} g\sqrt{j+1}(\lvert j+1\rangle\langle j\rvert a + \text{h.c.}). \quad (1)$$

Here, ω_r is the frequency of the bare resonator, $a^\dagger$ and a are the creation and annihilation operators for photons in the resonator, $\lvert j\rangle$ is the transmon state (which from here on is denoted by a number), ω_j is the eigenfrequency of the transmon's $\lvert j\rangle$ state, g is the coupling strength between the transmon and the resonator, and N_t is a cutoff for the number of transmon levels included in the simulations. The form of the transmon terms in the Hamiltonian is due to the transmon being an anharmonic oscillator [14].

Using the transmon and cavity parameters extracted from the spectroscopy, we calculate the (singly) dressed energy level diagram for the eigenstates. The result is listed in table 1. The main peaks observed in the probe scan range, at 6.61, 6.55, and 6.53 GHz (indicated by arrows 1–3 in figure 1(c)) correspond closely to the calculated frequency of the transitions in the dressed system $\lvert\mathbf{0}\rangle \leftrightarrow \lvert\mathbf{2}\rangle$, $\lvert\mathbf{1}\rangle \leftrightarrow \lvert\mathbf{4}\rangle$, and $\lvert\mathbf{3}\rangle \leftrightarrow \lvert\mathbf{7}\rangle$, respectively.

The observation of multiple peaks in the spectrum is indicative of a strong thermal population. If the system were in its ground state, only one peak, corresponding to the $\lvert\mathbf{0}\rangle \leftrightarrow \lvert\mathbf{2}\rangle$ transition, would be observed in this frequency range.

To further study the system, we apply a drive tone at frequency $\omega_d/2\pi$ to excite the system. As we scan the frequency of the drive tone, we observe splitting of the peaks in the probe spectrum at distinct frequencies. With increasing drive power, the splitting becomes more pronounced, and cross-like structures appear in the spectrum. Increasing drive power further causes new splittings to appear at different drive frequencies. These results are shown in the left panels of figures 2(a)–(c).
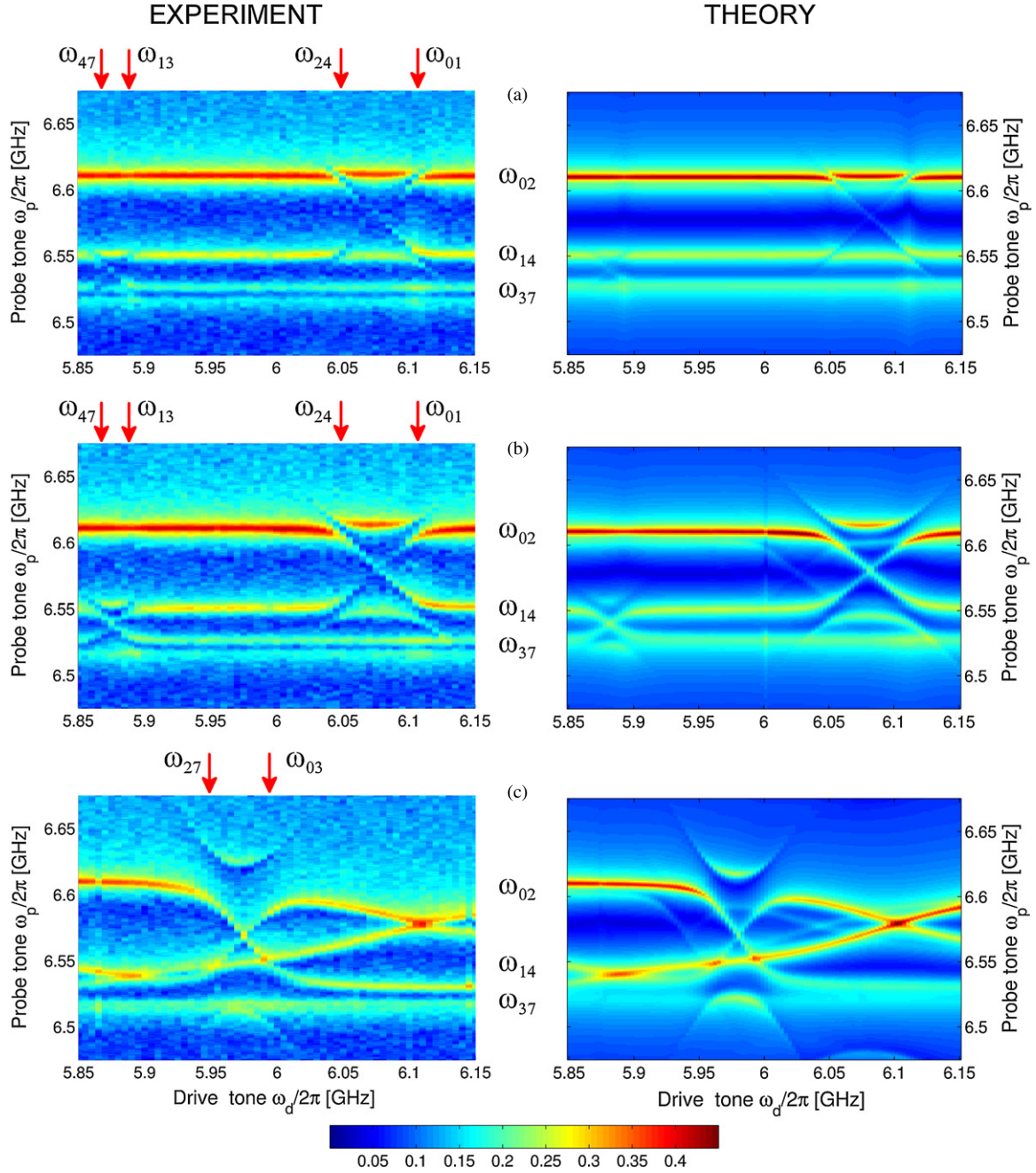
Figure 2. Measured (left) and modelled susceptibility (right) for the driven dressed system. Transitions are indicated by the red arrows. (a) Low drive power −110 dBm, (b) intermediate drive power −100 dBm, (c) high drive power −85 dBm. We use $N_t = 5$ transmon levels in the simulations. The only parameter changed in the model for the different cases is the number of drive photons in the resonator N_d. For both the experimental data and the calculated susceptibility we have plotted the square root of the magnitude. The square root is used to enhance some of the finer features of the response. In the theory plot, we have allowed drive strength $\xi_d = g_s\sqrt{N_d}$ to have a frequency dependence. Over the plotted frequency range ξ_d is increased by a factor of 3. This is consistent with driving the resonator off resonance over the considered frequency range.

To model the measured response, we add the drive term

$$H_{\mathrm{drive}} = \hbar \sum_{j=0}^{N_t-1} \xi_d \sqrt{j+1}(\mathrm{e}^{-\mathrm{i}\omega_d t}|j+1\rangle\langle j| + \mathrm{h.c.}) \quad (2)$$

to the Hamiltonian in equation (1). Here, we introduce the drive strength $\xi_d = g_s\sqrt{N_d}$, where N_d is the number of drive photons in the resonator and g_s is the coupling between a single drive photon in the resonator and the transmon.

We then calculate the susceptibility $\chi(\omega_p)$ of the cavity in response to a weak probe applied at the frequency $\omega_p/2\pi$ [22, 23]:

$$\chi(\omega_p) = \mathrm{i}\int_0^\infty \mathrm{d}t\, \mathrm{e}^{\mathrm{i}\omega_p t}\langle q(t)q(0) - q(0)q(t)\rangle, \quad (3)$$

where $q = a + a^\dagger$ is the voltage operator of the cavity. To calculate the expectation values in the integral, we first find the steady-state solution ρ_{ss} of the master equation

$$\dot{\rho} = \mathcal{L}\rho = -\frac{i}{\hbar}[H_{\text{rot}}, \rho] + \kappa N_\kappa \mathcal{D}[a^\dagger]\rho + \kappa(N_\kappa + 1)\mathcal{D}[a]\rho$$

$$+ \gamma N_\gamma \mathcal{D}\left[\sum_j \sqrt{j+1}|j+1\rangle\langle j|\right]\rho$$

$$+ \gamma(N_\gamma + 1)\mathcal{D}\left[\sum_j \sqrt{j+1}|j\rangle\langle j+1|\right]\rho$$

$$+ \frac{\gamma_\phi}{2}\mathcal{D}\left[\sum_j 2j|j\rangle\langle j|\right]\rho. \tag{4}$$

Here, H_{rot} is the total Hamiltonian from equations (1) and (2), moved to a frame rotating with the drive frequency ω_d, $\kappa = \omega_r/Q$ is the relaxation rate of the resonator, γ is the bare relaxation rate of the transmon, γ_ϕ is the pure dephasing rate of the transmon, $N_\gamma = 1/(\exp(\hbar\omega_{ge}/k_B T) - 1)$, $N_\kappa = 1/(\exp(\hbar\omega_r/k_B T) - 1)$, where T is the temperature of the bath, and $\mathcal{D}[X]\rho = X\rho X^\dagger - \frac{1}{2}X^\dagger X\rho - \frac{1}{2}\rho X^\dagger X$ is the Lindblad operator.

Noting that in this rotating frame, the expectation values from equation (3) can be expressed as [24]

$$\langle q(t)q(0)\rangle = \text{tr}\,(ae^{-i\omega_d t} + a^\dagger e^{i\omega_d t})e^{\mathcal{L}t}(a + a^\dagger)\rho_{ss} \tag{5}$$

$$\langle q(0)q(t)\rangle = \text{tr}\,(ae^{-i\omega_d t} + a^\dagger e^{i\omega_d t})e^{\mathcal{L}t}\rho_{ss}(a + a^\dagger), \tag{6}$$

we follow the method of [25] to calculate the susceptibility numerically.

Equation (3) gives the response of the voltage in the cavity due to a small external perturbation (i.e. the probe). Since the transmitted signal is proportional to the cavity voltage, χ is also proportional to the measured transmission coefficient, S_{21}.

In the experiment, we set the probe to -130 dBm at the sample. This is a level that gives a reasonable signal to noise without requiring a too long averaging time and appears weak enough not to alter the observed spectra. As we increase the drive power to about $+20$ dB above the probe, we begin to observe splittings of the transmission peaks at specific probe frequencies (figure 2(a)). As the drive power is increased even further ($+30$ dB above the probe), the transmission peaks split symmetrically, forming cross-like structures, shown in figure 2(b). The observed cross structures are accompanied by chevrons above and below, indicative of avoided level crossings. Increasing the power further to $+45$ dB above, the probe gives rise to additional cross structures; see figure 2(c).

We find that by calculating the susceptibility from equation (3) using parameters extracted for the system without a drive signal, we can reproduce the response of the system with a drive to a high degree of accuracy. This is shown in the right panels of figures 2(a)–(c). As we increase the drive power, the only parameter that is changed between these three plots is the number of drive photons (N_d) in the cavity. N_d is changed in the model to directly correspond to the increased drive power.

To understand the underlying processes that generate the cross structures in the spectra, we focus on the cross-like structure, with chevrons above and below, centred at $\omega_d/2\pi = 6.075$ GHz in figures 2(a) and (b) as an example.
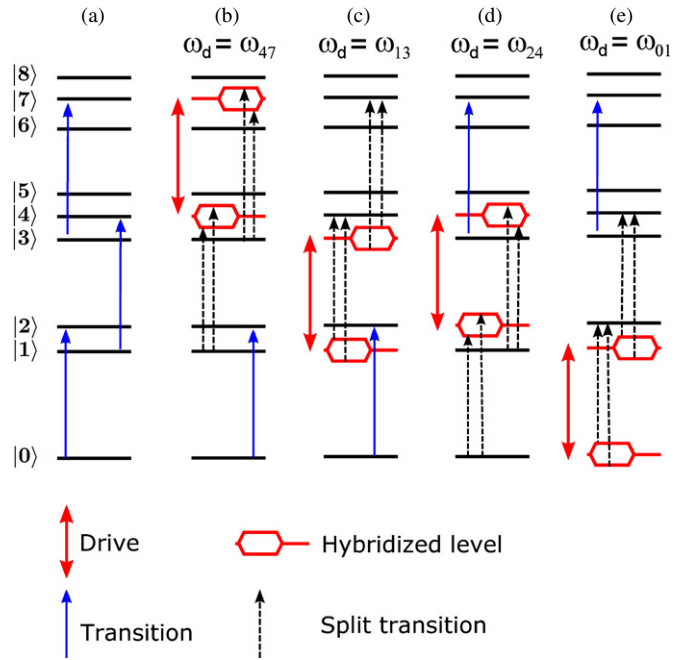

Figure 3. (a) Energy level diagram of the singly dressed qubit–resonator system. (b)–(e) illustrate driving the system on resonance with the transitions ω_{47}, ω_{13}, ω_{24} and ω_{01}. Solid red arrows indicate the drive, solid blue arrows indicate transitions unaffected by the drive, and dashed arrows indicate transitions split by the drive.

Here, the $|0\rangle \leftrightarrow |2\rangle$ and $|1\rangle \leftrightarrow |4\rangle$ transitions show splittings in the probe that merge in the centre. These splittings occur as the drive frequency is tuned through the $|2\rangle \leftrightarrow |4\rangle$ transition (indicated by ω_{24}) and then the $|0\rangle \leftrightarrow |1\rangle$ (indicated by ω_{01}). We understand this as follows: when the drive is resonant with the $|2\rangle \leftrightarrow |4\rangle$, the energy eigenstates $|2\rangle$ and $|4\rangle$ hybridize and split into two pairs of eigenstates separated by $\approx \pm\hbar\xi_d$ in energy. This in turn gives rise to the splitting of the $|0\rangle \leftrightarrow |2\rangle$ and $|1\rangle \leftrightarrow |4\rangle$ transitions. This is illustrated in figure 3 for the cases when ω_d is resonant with ω_{47}, ω_{13}, ω_{24} and ω_{01}. The last two cases let us understand the small cross seen around $\omega_d/2\pi = 5.88$ GHz in exactly the same way as we understand the large cross.

The reason why we observe a cross-like structure is that we are observing a process involving one drive photon and one probe photon. If we slightly detune the drive from say ω_{01}, we can still observe transmission peaks at $\omega_p = \omega_{12} - (\omega_{01} - \omega_d)$ and $\omega_p = \omega_{13} + (\omega_{01} - \omega_d)$, giving rise to the non-horizontal lines in the response. In general, a multi-photon process involving both drive and probe photons will lead to non-horizontal lines in the spectrum. To be more precise, a transition $|A\rangle \leftrightarrow |B\rangle$ will show up in the spectrum with a slope of $\pm n/m$ if $m\omega_p = \omega_{AB} \pm n\omega_d$.

For high drive powers, multi-photon processes become possible. This is illustrated by the crossing of the $|0\rangle \leftrightarrow |2\rangle$ and $|3\rangle \leftrightarrow |7\rangle$ transitions, shown in figure 2(c). This crossing is formed when two photons from the drive tone are absorbed/emitted as they go through the $|2\rangle \leftrightarrow |7\rangle$ (11.9/2 = 5.95 GHz) and $|0\rangle \leftrightarrow |3\rangle$ (12.00/2 = 6.00 GHz) transition. This results in a 3-photon (2 drive, 1 probe) process. Note how the increased number of drive photons involved

J. Phys. B: At. Mol. Opt. Phys. **46** (2013) 224014

A F Kockum *et al*

results in steeper slopes (compared to the cross in figures 2(a) and (b)) for the two lines making up this cross.

We also note that the energy splittings very closely follow a $\sqrt{N_d}$ dependence all the way from a splitting of 4 MHz up to a splitting of 73 MHz. At these drive powers, the coupling to the drive photons becomes comparable to the qubit–resonator coupling. The hybridized states hence represent true superposition states consisting of qubit states dressed by both the resonator and the drive, i.e., doubly dressed states. Another way to put it is that we are observing multiple instances of the Autler–Townes effect [26], where a strong drive dresses transitions (in our case, transitions between singly dressed states) and the new transitions between the split energy levels are detected by a weak probe tone. The Autler–Townes effect has been observed in several experiments with superconducting circuits over the last few years [27–30].

From the fits, we also extract an effective resonator bath temperature of ≈ 100 mK, and an effective qubit bath temperature of ≈ 400 mK, considerably higher than expected. The qubit bath temperature decreased slightly as the probe power was decreased, but full thermalization was not observed. One possible explanation is that the qubit thermalizes very slowly at low temperatures and hence does not thermalize fully during the limited hold time of the ADR (≈ 8 h). Another possibility is the presence of an infrared radiation background that prevents the qubit from reaching its ground state [31]. From the fit, we extract a T_1 of only 0.6 μs, significantly lower than the value extracted in [8] for a similar device. This suppression in T_1 is most likely due to the IR radiation, as previously observed [32].

In conclusion, we have investigated a strongly driven cQED system in the non-dispersive regime using a continuous readout, showing many rich features of the strongly coupled Jaynes–Cummings Hamiltonian. We model the response to a weak probe signal by calculating the susceptibility of the resonator, and find that the calculated response quantitatively reproduces the measured data. We explain the response in terms of multi-photon processes in the dressed basis.

Acknowledgments

References

[1] Berman P R (ed) 1994 *Cavity Quantum Electrodynamics* (New York: Academic)
[2] Raimond J M, Brune M and Haroche S 2001 *Rev. Mod. Phys.* **73** 556
[3] Blais A, Huang R-S, Wallraff A, Girvin S and Schoelkopf R 2004 *Phys. Rev.* A **69** 062320
[4] Wallraff A, Schuster D I, Blais A, Frunzio L, Majer J, Kumar S, Girvin S M and Schoelkopf R J 2004 *Nature* **431** 162
[5] Clarke J and Wilhelm F K 2008 *Nature* **453** 1031
[6] Niemczyk T *et al* 2010 *Nature Phys.* **6** 772
[7] Nakamura Y, Pashkin Y A and Tsai J S 1999 *Nature* **398** 786
[8] Sandberg M, Vissers M R, Ohki T A, Gao J, Aumentado J, Weides M and Pappas D P 2013 *Appl. Phys. Lett.* **102** 072601
[9] Paik H *et al* 2011 *Phys. Rev. Lett.* **107** 240501
[10] Rigetti C *et al* 2012 *Phys. Rev.* B **86** 100506
[11] Barends R *et al* 2013 arXiv:1304.2322v1
[12] Chang J *et al* 2013 *Appl. Phys. Lett.* at press arXiv:1303.4071v1
[13] Vissers M R, Gao J, Wisbey D S, Hite D A, Tsuei C C, Corcoles A D, Steffen M and Pappas D P 2010 *Appl. Phys. Lett.* **97** 232509
[14] Koch J, Yu T, Gambetta J, Houck A, Schuster D, Majer J, Blais A, Devoret M, Girvin S and Schoelkopf R 2007 *Phys. Rev.* A **76** 042319
[15] Gao J, Daal M, Vayonakis A, Kumar S, Zmuidzinas J, Sadoulet B, Mazin B A, Day P K and Leduc H G 2008 *Appl. Phys. Lett.* **92** 152505
[16] Sandberg M, Vissers M R, Kline J S, Weides M, Gao J, Wisbey D S and Pappas D P 2012 *Appl. Phys. Lett.* **100** 262605
[17] Wenner J *et al* 2011 *Appl. Phys. Lett.* **99** 113513
[18] Reed M, DiCarlo L, Johnson B, Sun L, Schuster D, Frunzio L and Schoelkopf R 2010 *Phys. Rev. Lett.* **105** 173601
[19] Bishop L S, Ginossar E and Girvin S M 2010 *Phys. Rev. Lett.* **105** 100505
[20] Boissonneault M, Gambetta J M and Blais A 2010 *Phys. Rev. Lett.* **105** 100504
[21] Fink J M, Baur M, Bianchetti R, Filipp S, Göppl M, Leek P J, Steffen L, Blais A and Wallraff A 2009 *Phys. Scr.* T **137** 014013
[22] Kubo R 1957 *J. Phys. Soc. Japan* **12** 570
[23] van Vliet K M 1978 *J. Math. Phys.* **19** 1345
[24] Gardiner C W and Zoller P 1991 *Quantum Noise* (Berlin: Springer)
[25] Rau I, Johansson G and Shnirman A 2004 *Phys. Rev.* B **70** 054521
[26] Autler S H and Townes C H 1955 *Phys. Rev.* **100** 703
[27] Sillanpää M A, Li J, Cicak K, Altomare F, Park J I, Simmonds R W, Paroanu G S and Hakonen P J 2009 *Phys. Rev. Lett.* **103** 193601
[28] Baur M, Filipp S, Bianchetti R, Fink J M, Göppl M, Steffen L, Leek P J, Blais A and Wallraff A 2009 *Phys. Rev. Lett.* **102** 243602
[29] Kelly W R, Dutton Z, Schlafer J, Mookerji B, Ohki T A, Kline J S and Pappas D P 2010 *Phys. Rev. Lett.* **104** 163601
[30] Li J, Paroanu G S, Cicak K, Altomare F, Park J I, Simmonds R W, Sillanpää M A and Hakonen P J 2012 *Sci. Rep.* **2** 645
[31] Barends R *et al* 2011 *Appl. Phys. Lett.* **99** 113507
[32] Corcoles A D, Chow J M, Gambetta J M, Rigetti C, Rozen J R, Keefe G A, Beth Rothwell M, Ketchen M B and Steffen M 2011 *Appl. Phys. Lett.* **99** 181906